# Realizing wide-temperature reversible Ca metal anodes through a $Ca^{2+}$-conducting artificial layer

*Zhen Hou[1], Rui Zhou[1], Zhiwen Min[2], Ziheng Lu[3,*], and Biao Zhang[1,*]*

[1]Department of Applied Physics, The Hong Kong Polytechnic University, Hung Hom, Hong Kong, China.

[2]Shenzhen Institutes of Advanced Technology, Chinese Academy of Sciences, Shenzhen 518055, China

[3]Microsoft Research AI4Science, Beijing 100080, China.

*Corresponding Author: zihenglu@microsoft.com; biao.ap.zhang@polyu.edu.hk

ABSTRACT: Room-temperature Ca deposition/stripping is impeded by the formation of ionic insulating interfaces. Electrolyte optimization could partly enhance Ca reversibility by tailoring the interfaces, but the precise regulation of the composition remains challenging. Herein, we turn to construct an ex-situ artificial layer on the Ca metal via a facile displacement reaction between metal halides and Ca. These Ca-driven spontaneous layers with precisely controlled interfacial chemistry consist of a Ca-metal alloy phase and a calcium halide matrix for conducting $Ca^{2+}$ and insulating the electrons, as revealed by theoretical and experimental investigations. In particular, the $Ca_{31}Sn_{20}/CaBr_2$ constituted interface enables Ca metal anodes with low polarization and humid air stability over a wide temperature range from -25 to 50 ºC. This proof-of-concept work provides

an alternative approach to boost $Ca^{2+}$ diffusivity through customized interfacial chemistry regulation.

## TOC GRAPHICS

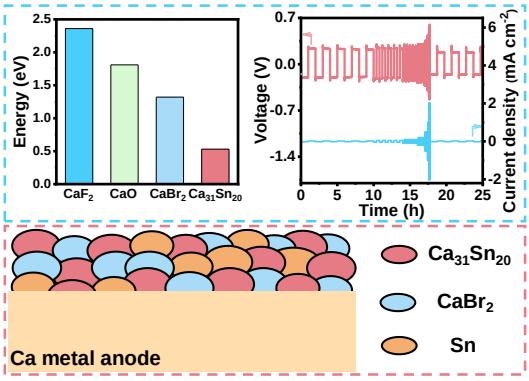


Multivalent-ion batteries (e.g., $Mg^{2+}$ and $Ca^{2+}$) are regarded as promising alternatives to conventional Li-ion batteries (LIBs) owing to the potential high energy gains arising from the multiple-electron redox chemistry.[1-7] Compare to Mg metal, Ca offers the significant advantages of the lower redox potential of -2.87 V vs. standard hydrogen electrode (SHE) and higher natural abundance.[8-12] Therefore, rechargeable Ca metal batteries (RCMBs) have attracted rising attention in recent years. However, their commercial application is long hindered by the formation of ionic insulating passivating films on Ca metal anodes in numerous aprotic-based electrolytes, which virtually impedes Ca reversibility.[12-17] Early work reports that $Ca(OH)_2$, $CaCO_3$, and calcium alkoxides are the main species in the passivating layers.[18]

Extensive efforts have been recently dedicated to screening electrolyte formulations for building ion-conducting solid electrolyte interphase (SEI).[19-25] In 2016, Ponrouch et al. constitute the first step towards reversible Ca electrodeposition at elevated temperature (75-100 ºC) using calcium

tetrafluoroborate $Ca(BF_4)_2$ in ethylene carbonate/propylene carbonate electrolyte.[19] Subsequently, a few electrolytes relying on special salts, such as calcium borohydride $Ca(BH_4)_2$[20] and calcium tetrakis(hexafluoroisopropyloxy)borate $Ca[B(hfip)_4]_2$[21,22], are reported to achieve room-temperature feasible Ca metal anodes. More recently, our group reveals that the solvents with high solvation capability benefit the formation of organic-rich SEIs for reversible Ca deposition/stripping.[26] Despite these encouraging progress, the precise manipulation of the composition and microstructure of SEI remains arduous owing to the intricate and obscure formation process, making it challenging to tailor the desired interface characteristics to further boost Ca metal anodes development explicitly.

Ex-situ construction of protective layers, which enables the precise and facile control of interfacial chemistry, is an alternative approach and has been proven effective in Li metal anodes.[27-29] Nevertheless, the extension of the strategy to Ca systems has rarely been explored. It remains unclear which phases have sufficient $Ca^{2+}$ conductivity and how to incorporate such phases into the interface. Herein, we construct a metal halide-derived interface on the top of Ca metal via a facile ion-exchange method, realizing low-polarization Ca metal anodes over a wide temperature range under a commercially available calcium bis(trifluoromethanesulfonyl)imide $Ca(TFSI)_2$-based electrolytes. Complementary experimental and theoretical studies reveal that the synergy of Ca-metal alloy phase (ion-conductor) and calcium halide matrix (electron-insulator) in the artificial layer contributes to the enhanced Ca reversibility.

Figure 1a illustrates the facile and scalable procedure to fabricate such an artificial layer onto Ca foil. Specifically, protected Ca metal anodes are obtained by drop-casting $SnBr_2$ solution onto polished Ca foils. The $SnBr_2$ is reduced to Sn, as confirmed by the X-ray diffraction (XRD) patterns and X-ray photoelectron spectroscopy (XPS) spectrum (Figure 1b,c). Part of Sn is further

alloyed with Ca to form a $Ca_{31}Sn_{20}$ phase (see Figure S1 for details). XPS also verifies the existence of $CaBr_2$ species by the peaks located at 68.9 and 69.9 eV in the Br 3d spectra (Figure 1d and Figure S2). Therefore, the artificial layer mainly consists of Sn metal, $Ca_{31}Sn_{20}$ alloy, and $CaBr_2$, which are formed according to the following reactions[27]:

$$Ca + SnBr_2 \rightarrow Sn + CaBr_2 \quad (1)$$

$$31\ Ca + 20\ Sn \rightarrow Ca_{31}Sn_{20} \quad (2)$$

Scanning electron microscopy (SEM) images show the artificial layer has a relatively smooth structure consisting of tiny particles (Figure 1e,f and Figure S3). The corresponding energy dispersive spectroscopy (EDS) elemental mapping demonstrates evenly distributed Sn and Br elements throughout the artificial layer (Figure 1g,h). The thickness is around 1 um, as measured from the cross-sectional SEM images (Figure S4).

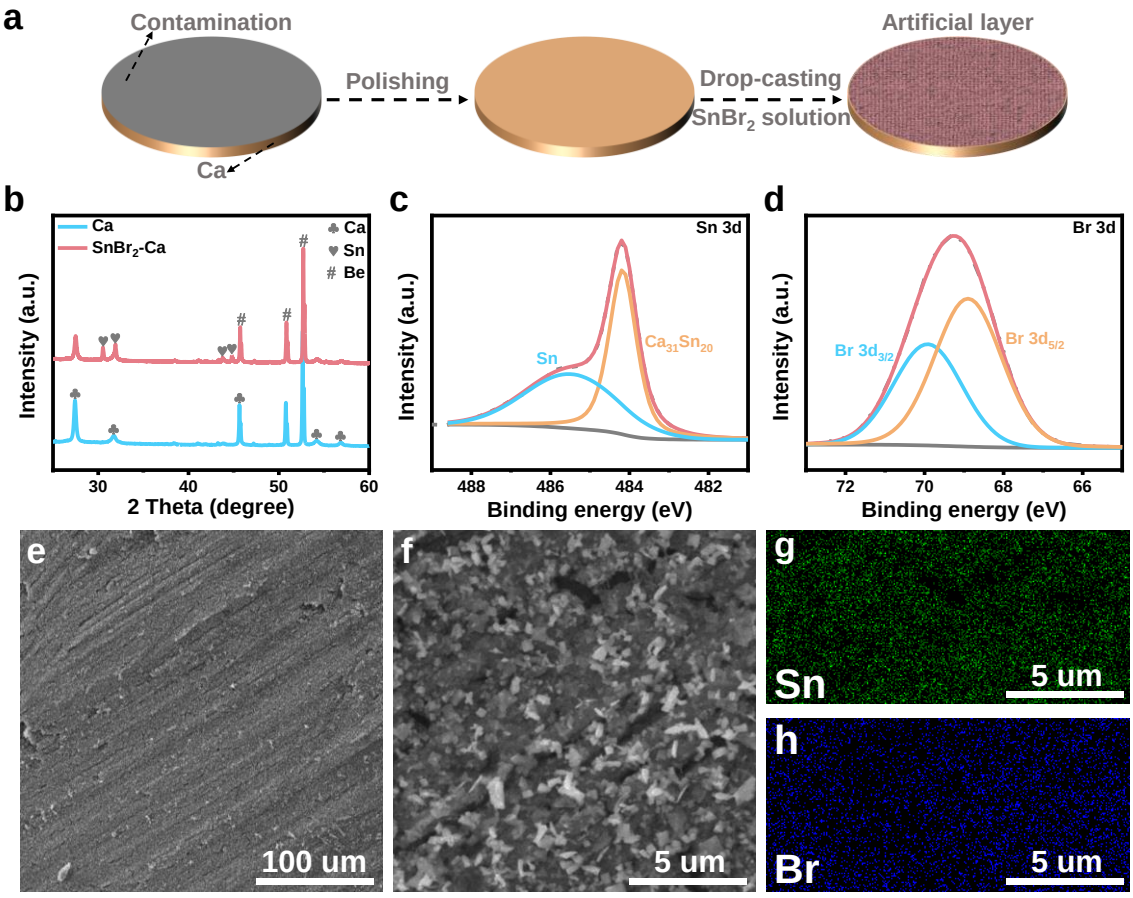


Figure 1. Preparation of the artificial layer. (a) Synthesis procedure. (b) XRD patterns of Ca and $SnBr_2$-Ca. Note that the tested samples are loaded on the Swagelok cell equipped with a Be window for avoiding oxidation, which brings about the Be signals. XPS spectra of (c) Sn 3d and (d) Br 3d after Ar ion sputtering of 150 s. (e,f) Top-view SEM images of $SnBr_2$-Ca. (g,h) The corresponding EDS elemental mapping of top-half of f.

We collect the EIS of the symmetric cells using either pristine Ca or modified Ca (denoted as $SnBr_2$-Ca) as the electrodes to examine the effect of the artificial interface. The adopted electrolyte is 0.1 M $Ca(TFSI)_2$ in strongly-solvating dimethylacetamide (DMAc) that has been reported to support reversible Ca deposition/stripping,[26] but the kinetics requires further improvements to

decrease the large overpotential due to the absence of effective ionic conductive phases. As shown in Figure 2a, large interfacial resistance of ~700 kΩ is observed in pristine Ca. By contrast, the value decreases by an order of magnitude (~25 kΩ) when $SnBr_2$-Ca is applied, proving the beneficial roles of the artificial layer in promoting $Ca^{2+}$ transport. Cyclic voltammograms (CV) are further carried out to investigate Ca deposition/stripping behavior. A small redox current is detected with bare Ca electrodes (Figure 2b). In comparison, reversible Ca deposition/stripping with a current up to 0.8 mA $cm^{-2}$ is observed with the assistance of the artificial layer. Besides, the peak current maintains after 200 repeated deposition/stripping cycles, reflecting its excellent stability and durability during cycling. This is further proved by the XPS spectra of cycled $SnBr_2$-Ca where artificial layer remains onto $SnBr_2$-Ca (Figure S5).

To exclude the artifact from the side reactions, we track the redox potential of $SnBr_2$-Ca during cycling by an $Ag/Ag^+$ reference electrode in a Swagelok-type three-electrode cell configuration (Figure S6), where $SnBr_2$-Ca is adopted as the working electrode and counter electrode. The $Ag/Ag^+$ reference electrode is calibrated with an internal reference redox couple of ferrocene/ferrocenium ($Fc/Fc^+$). The calculated potential of $SnBr_2$-Ca is -2.62 V vs. SHE at open-circuit voltage, 0.25 V shift compared to -2.87 V vs. SHE which is evaluated in an aqueous solution. Such discrepancy originates mainly from solvation differences under organic and aqueous electrolytes, widely observed in Li/Na/K metal anodes.[30,31] The three-electrode cell is discharged/charged at 0.1 mA $cm^{-2}$ for 2 h to allow a real-time monitor of its deposition/stripping potential. Ca deposition/stripping starts at -2.87/-2.52 V vs. SHE in 1$^{st}$ cycle (Figure 2c), resulting in an overpotential of 0.35 V, which agrees well with the data measured in symmetric two-electrode coin cells (Figure S7c).

$SnBr_2$-Ca|$SnBr_2$-Ca symmetric cells are assembled to examine the cyclic stability under 0.02 mA $cm^{-2}$ with deposition/stripping for 1 h each cycle. It displays a stable voltage profile of more than 700 h with a low overpotential of ~0.25 V compared to ~0.60 V for the bare Ca electrode (Figure 2d). Decent deposition/stripping is sustained at a large cycling capacity of 1 mAh $cm^{-2}$ by increasing deposition/stripping time to 50 h, which rules out the possibility of charge storage provided by alloying/dealloying reaction of $Ca_{31}Sn_{20}$ (see Figure S7 for details). In addition, $SnBr_2$-Ca delivers a promising rate performance (Figure 2e), maintaining the reversibility at a high current density up to 2 mA $cm^{-2}$. We also investigate its stability under harsh environments. Interestingly, the cells could be stably operated for 500 h at 0 and 50 $^oC$ (Figure 2f). Pushing to the limit, a 250 h lifetime could be maintained even at -25 $^oC$. It is worth mentioning that low-temperature Ca deposition/stripping has never been achieved due to the poor reaction kinetics. Another asset of the artificial interface is the increased stability in ambient air with high relative humidity (RH) of ~60%. After exposure to the air for 6 h, the $SnBr_2$-Ca still delivers a stable cycle of 300 h with a low overpotential of ~0.50 V (Figure 2g). Without the protective interface, the bare Ca is rapidly oxidized as inferred by the surface color change (Figure S8), and the performance is severely degraded. The compatibility of the artificial interface with other electrolytes is evaluated by either replacing the $Ca(TFSI)_2$ with $Ca(FSI)_2$ and $Ca(CF_3SO_3)_2$ salts or changing DMAc to another strongly-solvating solvents (e.g., 1-methylimidazole (MeIm) and triethyl phosphate (TEP)). In both cases, the $SnBr_2$-Ca electrode shows much-improved performance compared to bare Ca (Figure S9 and S10), manifesting a broad application of the artificial layer.

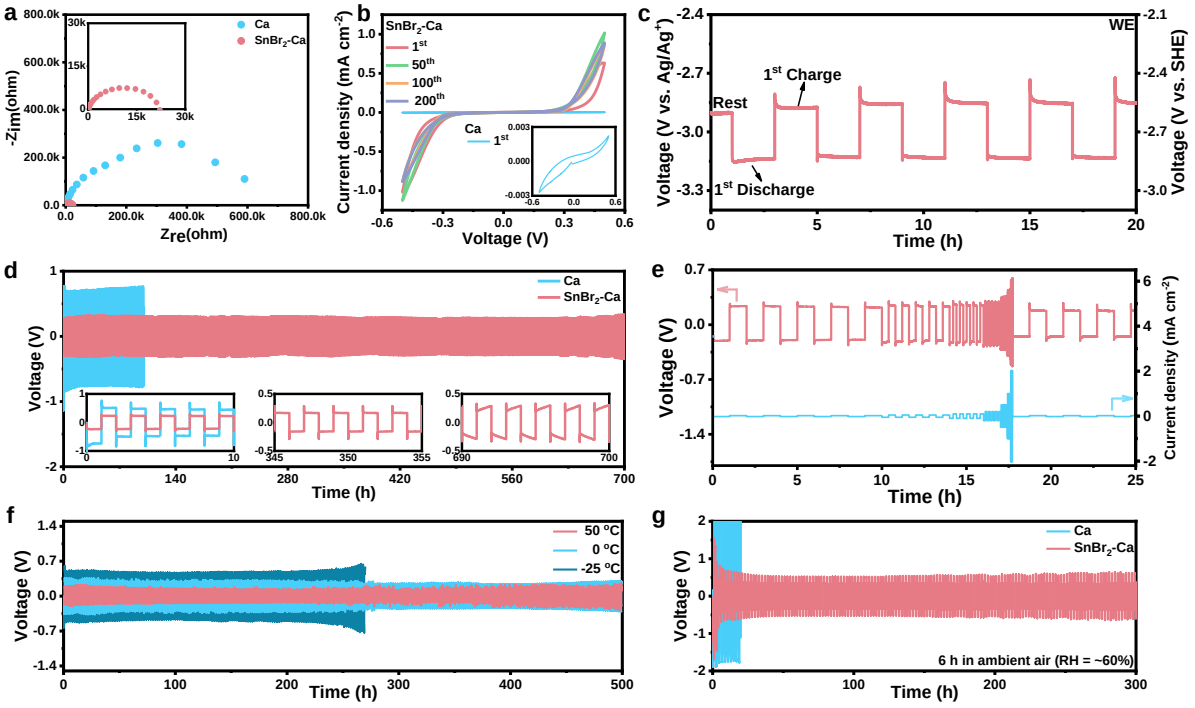


Figure 2. Electrochemical performance of $SnBr_2$-Ca|$SnBr_2$-Ca symmetric cells. (a) EIS. (b) CVs at a scan rate of 10 mV $s^{-1}$ between -0.5 and 0.5 V. (c) Ca deposition/stripping curve in $SnBr_2$-Ca electrode with the potential calibrated. (d) Cycling performance at 0.02 mA $cm^{-2}$. (e) Rate capability at 0.02, 0.05, 0.1, 0.2, 0.5, 1 and 2 mA $cm^{-2}$. Cycling performance at 0.02 mA $cm^{-2}$ (f) under thermal extremes, and (g) with Ca and $SnBr_2$-Ca metal anodes exposed to ambient air for 6 h.

Having demonstrated the enhanced $Ca^{2+}$ diffusion in the artificial layer, density functional theory (DFT) simulations are conducted to examine which induced phases are $Ca^{2+}$ conductive. As shown in Figure 3a-c and Figure S11, we calculate the $Ca^{2+}$ diffusion energy barriers in bulk $Ca_{31}Sn_{20}$ and $CaBr_2$ and compare them with those in $CaF_2$ and CaO, which are the main inorganic component in most SEIs. It is observed that $Ca_{31}Sn_{20}$ and $CaBr_2$ display significantly lower $Ca^{2+}$ diffusion barriers. In particular, the $Ca_{31}Sn_{20}$ shows a small $Ca^{2+}$ diffusion barrier of 0.53 eV,

which is considerably lower than that in the known $Ca^{2+}$-insulating $CaF_2$ phase with a barrier of 2.36 eV. This observation indicates that $Ca_{31}Sn_2$ should be responsible for $Ca^{2+}$ conduction in the artificial layer. On the other hand, according to the previous studies,[27,32,33] the electron-insulator $CaBr_2$ phase is expected to build a necessary potential gradient across the layer to ensure $Ca^{2+}$ diffusion through the film. This could be confirmed by the direct current-voltage results of $SnBr_2$-Ca and Sn-Ca. The electronic resistivity of $SnBr_2$-Ca is about one order of magnitude larger than that of Sn-Ca, leading to enhanced cyclic stability (see Figure S12 for details).

Based on these observations, we depict the working mechanism of the artificial layer (Figure 3d). Protogenetic SEI, which consists of an amorphous polymer matrix with minor CaO and $CaF_2$ particles embedded[26], merely allows slow $Ca^{2+}$ diffusion due to the absence of effective ionic conductive phases, leading to a large polarization during the Ca deposition/stripping process. By contrast, the construction of an artificial layer (including ion-conductor $Ca_{31}Sn_2$ and electron-insulator $CaBr_2$) could significantly promote $Ca^{2+}$ mobility, enabling low-polarization Ca metal anodes during long-term cycling. Such an interface could be readily prepared through the Ca surface treatment with metal halides, which have a vast family for further optimization. As a proof-of-concept, we generalize this approach to the other metal halides. We first focus on another tin halide ($SnCl_2$) to explore the effects of calcium halides and then turn to other metal bromides, such as $SbBr_3$ and $BiBr_3$, to examine the roles of Ca alloys. The metals, i.e., Sb and Bi, are selected from those that could alloy with Ca according to the previous experimental and theoretical studies.[34,35] It is a delight to find that all three protective layers could benefit the reversible Ca deposition/stripping to different extents (Figure S13). The results confirm the favorable metal halide-derived artificial interface in boosting the reversibility of Ca metal anodes. Further studies may follow this promising roadmap by optimizing the composition and microstructure.

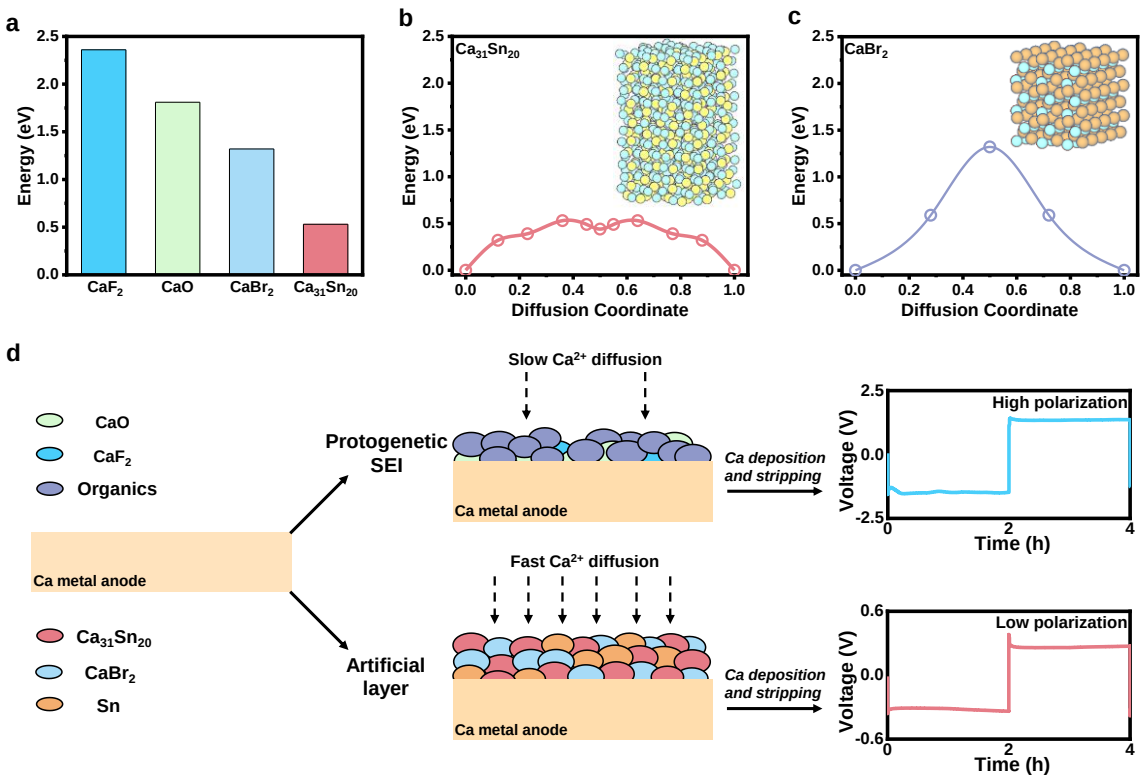


Figure 3. Working mechanism of artificial layer. (a-c) The calculated diffusion energy barriers in $CaF_2$, CaO, $CaBr_2$ and $Ca_{31}Sn_{20}$ bulk crystal. It is worth noting that the chance for the diffusion of $Ca^{2+}$ in the pure Sn phase is slim because of the tightly packed Sn atomic structure, and an alloying reaction front pushes the reaction. (d) Illustrations of deposition/stripping behavior without and with the artificial layer. The deposition/stripping curves are originated from Figure S7c.

Last, we assess the feasibility and durability of the artificial interface by pairing the $SnBr_2$-Ca electrode with the graphite electrode in 0.1 M $Ca(TFSI)_2$/DMAc electrolytes (Figure 4a). Graphite electrode has been reported to be a promising electrode for RCMBs.[36,37] Without artificial interface, the pristine Ca-graphite cell shows a large polarization with limited cycle life (Figure S14). In comparison, the $SnBr_2$-Ca|graphite cell could be reversibly discharged/charged at 100 mA $g^{-1}$ over 100 cycles (Figure 4b and Figure S15), delivering a discharge capacity of ~75 mAh $g^{-1}$.

The charge is stored through the solvent co-intercalation to form a ternary graphite intercalation compounds (GICs). Various intermediate GICs with different stages could be presented[37], leading to the multi-plateaus in the discharge/charge curves. The calciation behavior in graphite electrodes is confirmed by Raman spectra and EDS elemental mappings (Figure S16). These results prove the reliability of the $SnBr_2$-Ca electrode.

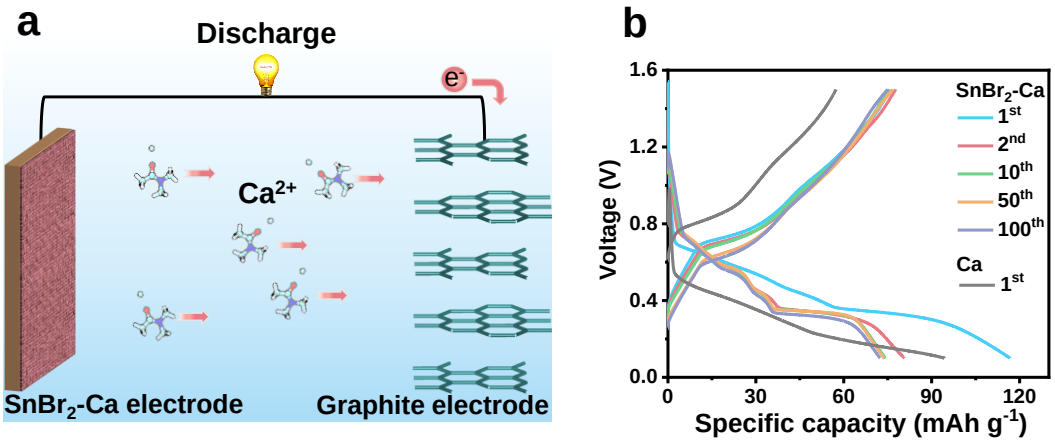


Figure 4 $SnBr_2$-Ca|graphite cell demonstration. (a) Work schematic during the discharge process. (b) Voltage profiles of the cell at 100 mA $g^{-1}$.

In summary, we report that Ca metal anodes with superior reversibility, low polarization and humid air stability over a wide temperature range from -25 to 50 ºC through ex-situ regulating electrode/electrolyte interfacial chemistry. Specifically, simple ion-exchange chemistry between Ca and $SnBr_2$ is employed to construct an artificial layer consisting of Sn metal/alloy and $CaBr_2$. The former, serving as an ion-conductor, offers a pathway for $Ca^{2+}$ transport. The latter acting as an electron-insulator prevents the reduction of $Ca^{2+}$ on the surface and provides a driving force for $Ca^{2+}$ deposition under the artificial layer. Furthermore, as a proof of concept, $SnBr_2$-Ca/graphite cell is reversibly operated in commercially available $Ca(TFSI)_2$-based electrolyte. This work offers

fertile ground for exploring ex-situ $Ca^{2+}$ conducting protective layers on Ca anode, where metal halides display merits in building such layers.

## ASSOCIATED CONTENT

### Supporting Information

The Supporting Information is available free of charge on the ACS Publications website.

Experimental section; additional data from XPS, XRD and SEM; cycling performance of other modified Ca metal anodes or $SnBr_2$-Ca using electrolyte with other salts; electronic conductivities of $SnBr_2$-Ca and Sn-Ca; calciation/decalciation behavior in graphite electrodes; Swagelok-based three-electrode cell setup; optical images of Ca and $SnBr_2$-Ca in ambient air; diffusion barrier of $Ca^{2+}$ in CaO and $CaF_2$ bulk crystal.

## AUTHOR INFORMATION


### Corresponding Author

Ziheng Lu- Microsoft Research AI4Science, Beijing, China; E-mail: zihenglu@microsoft.com; orcid.org/0000-0001-8687-8946

Biao Zhang-Department of Applied Physics, The Hong Kong Polytechnic University, Hung Hom, Hong Kong, China; E-mail: biao.ap.zhang@polyu.edu.hk; orcid.org/0000-0003-2239-8526

### Author

Zhen Hou-Department of Applied Physics, The Hong Kong Polytechnic University, Hung Hom, Hong Kong, China; orcid.org/0000-0002-0939-6115

Rui Zhou-Department of Applied Physics, The Hong Kong Polytechnic University, Hung Hom, Hong Kong, China

Zhiwen Min-Shenzhen Institutes of Advanced Technology, Chinese Academy of Sciences, Shenzhen 518055, China

Author Contributions

B.Z. and Z.H. conceived the idea and designed the experiments. Z.H. performed material characterizations and electrochemical measurements. R.Z. carried out XRD test. Z.L. and Z.M. conducted theoretical calculations. B.Z. and Z.H. analyzed the data, and prepared this manuscript with inputs from Z.L.

Notes

The authors declare no competing financial interest.

ACKNOWLEDGMENT

This work was supported by the General Research Fund (GRF) scheme of the Hong Kong Research Grants Council (Project No. 15306422). Z.L. thanks the Bin Shao and Tie-Yan Liu from Microsoft Research for the help in computational resources. We are grateful to Prof. J.M. Tarascon for offering valuable comments on this work.

REFERENCES

(1) Liang, Z.; Ban, C., Strategies to enable reversible magnesium electrochemistry: from electrolytes to artificial solid-electrolyte interphases. *Angew. Chem. Int. Ed.* **2021,** *60*, 11036-11047.

(2) Arroyo-de Dompablo, M. E.; Ponrouch, A.; Johansson, P.; Palacin, M. R., Achievements, challenges, and prospects of calcium batteries. *Chem. Rev.* **2020,** *120*, 6331-6357.

(3) Muldoon, J.; Bucur, C. B.; Gregory, T., Quest for nonaqueous multivalent secondary batteries: magnesium and beyond. *Chem. Rev.* **2014,** *114*, 11683-720.
(4) Wang, M.; Jiang, C.; Zhang, S.; Song, X.; Tang, Y.; Cheng, H. M., Reversible calcium alloying enables a practical room-temperature rechargeable calcium-ion battery with a high discharge voltage. *Nat. Chem.* **2018,** *10*, 667-672.
(5) Zhao-Karger, Z.; Xiu, Y.; Li, Z.; Reupert, A.; Smok, T.; Fichtner, M., Calcium-tin alloys as anodes for rechargeable non-aqueous calcium-ion batteries at room temperature. *Nat. Commun.* **2022,** *13*, 3849.
(6) Li, Y.; Lu, Y.; Adelhelm, P.; Titirici, M.-M.; Hu, Y.-S., Intercalation chemistry of graphite: alkali metal ions and beyond. *Chem. Soc. Rev.* **2019,** *48*, 4655-4687.
(7) Shterenberg, I.; Salama, M.; Yoo, H. D.; Gofer, Y.; Park, J.-B.; Sun, Y.-K.; Aurbach, D., Evaluation of $(CF_3SO_2)_2N$-(TFSI) based electrolyte solutions for Mg batteries. *J. Electrochem. Soc.* **2015,** *162*, A7118.
(8) Gummow, R. J.; Vamvounis, G.; Kannan, M. B.; He, Y., Calcium-ion batteries: current state-of-the-art and future perspectives. *Adv. Mater.* **2018,** *30*, e1801702.
(9) Nielson, K. V.; Liu, T. L., Dawn of calcium batteries. *Angew. Chem. Int. Ed.* **2020,** *59*, 3368-3370.
(10) Hosein, I. D., The promise of calcium batteries: open perspectives and fair comparisons. *ACS Energy Lett.* **2021**, 1560-1565.
(11) Gao, X.; Liu, X.; Mariani, A.; Elia, G. A.; Lechner, M.; Streb, C.; Passerini, S., Alkoxy-functionalized ionic liquid electrolytes: understanding ionic coordination of calcium ion speciation for the rational design of calcium electrolytes. *Energy Environ. Sci.* **2020,** *13*, 2559-2569.
(12) McClary, S. A.; Long, D. M.; Sanz-Matias, A.; Kotula, P. G.; Prendergast, D.; Jungjohann, K. L.; Zavadil, K. R., A heterogeneous oxide enables reversible calcium electrodeposition for a calcium battery. *ACS Energy Lett.* **2022,** *7*, 2792-2800.
(13) Ji, B.; He, H.; Yao, W.; Tang, Y., Recent advances and perspectives on calcium-ion storage: key materials and devices. *Adv. Mater.* **2021,** *33*, e2005501.
(14) Forero-Saboya, J.; Davoisne, C.; Dedryvère, R.; Yousef, I.; Canepa, P.; Ponrouch, A., Understanding the nature of the passivation layer enabling reversible calcium plating. *Energy Environ. Sci.* **2020,** *13*, 3423-3431.
(15) Staniewicz, R. J., A study of the calcium-thionyl chloride electrochemical system. *J. Electrochem. Soc.* **1980,** *127*, 782.
(16) Driscoll, D. M.; Dandu, N. K.; Hahn, N. T.; Seguin, T. J.; Persson, K. A.; Zavadil, K. R.; Curtiss, L. A.; Balasubramanian, M., Rationalizing calcium electrodeposition behavior by quantifying ethereal solvation effects on $Ca^{2+}$ coordination in well-dissociated electrolytes. *J. Electrochem. Soc.* **2020,** *167*, 160512.
(17) Melemed, A. M.; Gallant, B. M., Electrochemical signatures of interface-dominated behavior in the testing of calcium foil anodes. *J. Electrochem. Soc.* **2020,** *167*, 140543.
(18) Aurbach, D.; Skaletsky, R.; Gofer, Y., The electrochemical-behavior of calcium electrodes in a few organic electrolytes. *J. Electrochem. Soc.* **1991,** *138*, 3536-3545.
(19) Ponrouch, A.; Frontera, C.; Barde, F.; Palacin, M. R., Towards a calcium-based rechargeable battery. *Nat. Mater.* **2016,** *15*, 169-72.
(20) Wang, D.; Gao, X.; Chen, Y.; Jin, L.; Kuss, C.; Bruce, P. G., Plating and stripping calcium in an organic electrolyte. *Nat. Mater.* **2018,** *17*, 16-20.
(21) Li, Z.; Fuhr, O.; Fichtner, M.; Zhao-Karger, Z., Towards stable and efficient electrolytes for room-temperature rechargeable calcium batteries. *Energy Environ. Sci.* **2019,** *12*, 3496-3501.

(22) Shyamsunder, A.; Blanc, L. E.; Assoud, A.; Nazar, L. F., Reversible calcium plating and stripping at room temperature using a borate salt. *ACS Energy Lett.* **2019,** *4*, 2271-2276.
(23) Kisu, K.; Kim, S.; Shinohara, T.; Zhao, K.; Zuttel, A.; Orimo, S. I., Monocarborane cluster as a stable fluorine-free calcium battery electrolyte. *Sci. Rep.* **2021,** *11*, 7563.
(24) Song, H.; Su, J.; Wang, C., Hybrid solid electrolyte interphases enabled ultralong life Ca-metal batteries working at room temperature. *Adv. Mater.* **2021,** *33*, e2006141.
(25) Jie, Y.; Tan, Y.; Li, L.; Han, Y.; Xu, S.; Zhao, Z.; Cao, R.; Ren, X.; Huang, F.; Lei, Z.; Tao, G.; Zhang, G.; Jiao, S., Electrolyte Solvation Manipulation Enables Unprecedented room-temperature calcium-metal batteries. *Angew. Chem. Int. Ed.* **2020,** *59*, 12689-12693.
(26) Hou, Z.; Zhou, R.; Yao, Y.; Min, Z.; Lu, Z.; Zhu, Y.; Tarascon, J.; Zhang, B.; Correlation between electrolyte chemistry and solid electrolyte interphase for reversible Ca metal anodes. *Angew. Chem. Int. Ed.* **2022**, e202214796.
(27) Liang, X.; Pang, Q.; Kochetkov, I. R.; Sempere, M. S.; Huang, H.; Sun, X.; Nazar, L. F., A facile surface chemistry route to a stabilized lithium metal anode. *Nat. Energy* **2017,** *2*, 17119.
(28) Yourey, W.; Weinstein, L.; Halajko, A.; Amatucci, G. G., Pathways to enabling solid state electrolytically formed batteries: the solid electrolyte interphase. *Electrochim. Acta* **2012,** *66*, 193-203.
(29) Hou, Z.; Zhang, J.; Wang, W.; Chen, Q.; Li, B.; Li, C., Towards high-performance lithium metal anodes via the modification of solid electrolyte interphases. *J. Energy Chem.* **2020,** *45*, 7-17.
(30) Komaba, S.; Hasegawa, T.; Dahbi, M.; Kubota, K., Potassium intercalation into graphite to realize high-voltage/high-power potassium-ion batteries and potassium-ion capacitors. *Electrochem. Commun.* **2015,** *60*, 172-175.
(31) Marcus, Y., Thermodynamic functions of transfer of single ions from water to nonaqueous and mixed solvents: Part 3-standard potentials of selected electrodes. *Pure Appl. Chem.* **1985,** *57*, 1129-1132.
(32) Zhao, Y.; Du, A.; Dong, S.; Jiang, F.; Guo, Z.; Ge, X.; Qu, X.; Zhou, X.; Cui, G., A bismuth-based protective layer for magnesium metal anode in noncorrosive electrolytes. *ACS Energy Lett.* **2021,** *6*, 2594-2601.
(33) Lv, R.; Guan, X.; Zhang, J.; Xia, Y.; Luo, J., Enabling Mg metal anodes rechargeable in conventional electrolytes by fast ionic transport interphase. *Natl. Sci. Rev.* **2020,** *7*, 333-341.
(34) Ouchi, T.; Kim, H.; Spatocco, B. L.; Sadoway, D. R., Calcium-based multi-element chemistry for grid-scale electrochemical energy storage. *Nat. Commun.* **2016,** *7*, 10999.
(35) Yao, Z.; Hegde, V. I.; Aspuru‐Guzik, A.; Wolverton, C., Discovery of calcium-metal alloy anodes for reversible Ca-ion batteries. *Adv. Energy Mater.* **2019,** *9*, 1802994.
(36) Richard Prabakar, S. J.; Ikhe, A. B.; Park, W. B.; Chung, K. C.; Park, H.; Kim, K. J.; Ahn, D.; Kwak, J. S.; Sohn, K. S.; Pyo, M., Graphite as a long-life $Ca^{2+}$-intercalation anode and its implementation for rocking-chair type calcium-ion batteries. *Adv. Sci.* **2019,** *6*, 1902129.
(37) Park, J.; Xu, Z. L.; Yoon, G.; Park, S. K.; Wang, J.; Hyun, H.; Park, H.; Lim, J.; Ko, Y. J.; Yun, Y. S.; Kang, K., Stable and high-power calcium-ion batteries enabled by calcium intercalation into graphite. *Adv. Mater.* **2020,** *32*, e1904411.